Insights into a Mutation-Assisted Lateral Drug Escape Mechanism from the HIV-1 Protease Active Site†

S. Kashif Sadiq, Shunzhou Wan, and Peter V. Coveney*

Centre for Computational Science, Department of Chemistry, University College London, London, WC1H 0AJ, U.K.

Received May 9, 2007; Revised Manuscript Received October 11, 2007

ABSTRACT: We provide insight into the first stages of a kinetic mechanism of lateral drug expulsion from the active site of HIV-1 protease, by conducting all atom molecular dynamics simulations with explicit solvent over a time scale of 25 ns for saquinavir bound to the wildtype, G48V, L90M and G48V/L90M mutant proteases. We find a consistent escape mechanism associated with the G48V mutation. First, increased hydrophilic and hydrophobic flap coupling and water mediated disruption of catalytic dyad hydrogen bonding induce drug motion away from the dyad and promote protease flap transition to the semi-open form. Conversely flap-inhibitor motion is decoupled in the wildtype. Second, the decrease of total interactions causes unidirectional lateral inhibitor translation by up to 4 Å toward the P3 subsite exit of the active site, increased P3 subsite exposure to solvent and a complete loss of hydrophobic interactions with the opposite end of the active site. The P1 subsite moves beyond the hydrophobic active site side pocket, the only remaining steric barrier to complete expulsion being the "breathable" residue, P81. Significant inhibitor deviation is reported over 25 ns, and subsequent complete expulsion, implemented using steered molecular dynamics simulations, is shown to occur most easily for the G48V-containing mutants. Our simulations thus provide compelling support for lateral drug escape from a protease in a semi-open flap conformation. It is likely that some mutations take advantage of this escape mechanism to increase the rate of inhibitor dissociation from the protease. Finally, unidirectional translation may be countered by designing inhibitors with terminal subsites that provide sufficient anchoring to the flaps, thus increasing the steric barrier for translation in either direction.

Overcoming the development of inhibitor induced resistance by the human immuno deficiency virus (HIV[1]) remains one of the greatest challenges in the struggle against AIDS. The aspartyl protease synthesized by HIV is a homodimer with *C*2-symmetry, composed of 99 amino acids in each chain. The active site of the enzyme is formed by the dimer interface with an aspartic acid from each chain at the base, enclosed by a pair of hairpin β-sheets known as the "flaps". Due to its key role in the cleavage and subsequent maturation of the matrix (gag) and enzymatic (pol) proteins from their precursors, the protease has been a key target for structure-based antiretroviral inhibitors (*1*, *2*). Unfortunately, the high replication rate of the virus and low fidelity of the reverse transcription process have led to the proliferation of several resistant strains that follow emerging mutational patterns (*3*−*6*).

The loss in binding affinity of inhibitors to drug resistant mutants of HIV-1 protease as compared to the wildtype has been very well studied experimentally (*7*−*9*) and computationally (*10*−*12*). However, such calculations do not provide information about the kinetic mechanism of drug association or dissociation, nor can they alone explain the variation in the kinetic role of mutations in causing resistance.

For example, while it is likely that some active site mutations like V82A and I84V cause resistance through direct steric hindrance, other mutations not in the active site cause resistance through an alteration in the dynamical properties of the enzyme (*13*, *14*). Furthermore, for some such mutations, although structural differences between proteases remain small, significantly different clinical behavior is observed (*15*).

The role of the flaps in the catalytic mechanism of HIV-1 protease has been extensively studied. Ligands bind to the protease in a two-step binding process, first forming a loose complex, with the flaps in an open conformation, and second with the flaps securing the ligand in a closed conformation (*16*). Previous studies of the many crystal structures reported for HIV protease complexes have revealed the characteristic flexibility of the flaps together with the stability of the catalytic region (*17*). Furthemore, the crystal structures of

† We are grateful to EPSRC for funding much of this research through RealityGrid Grant GR/R67699, which provided access to the U.K. national supercomputing resources of CSAR in Manchester and HPCx in Daresbury. The Ph.D. studentship of S.K.S. is also funded by EPSRC. Our work was partially supported by the National Science Foundation under NRAC Grant MCA04N014, utilizing the TeraGrid cluster at the National Computational Science Alliance. This research has also been partially supported by the EU-funded ViroLab project (IST-027446).

* Corresponding author. Address: Centre for Computational Science, Department of Chemistry, University College London, 20 Gordon Street, London, WC1H 0AJ, U.K. Tel: +44 (0) 207 679 4560. Fax: +44 (0) 207 679 7463. E-mail: p.v.coveney@ucl.ac.uk.

[1] Abbreviations: HIV, human immunodeficiency virus; PCA, principal component analysis; SMD, steered molecular dynamics; RMSD, root-mean-squared deviation.

10.1021/bi700864p CCC: $40.75
Published on Web 00/00/0000 PAGE EST: 12.5

apo-proteases are almost entirely in a third, semi-open flap conformation, while ligand-bound structures are predominantly in a closed conformation.

Protease flexibility, stability and flap motion have also been extensively studied using computational techniques such as molecular dynamics (*18*−*20*) Recent studies on both the free and inhibitor-bound enzyme suggest the predominance of the semi-open flap conformation in the unliganded protease which can repeatedly open and close, while showing that the flaps remain stably closed when an inhibitor is bound (*21*). This is in good agreement with previous NMR studies (*22*, *23*) that have suggested equilibria between open, semi-open and closed forms of the flaps. Interestingly, a recent crystal structure of an unbound multi-drug resistant (MDR) protease with flaps in an open conformation was found to revert back to a semi-open form in molecular dynamics simulations (*24*), and it was suggested that such an open form was due to crystal packing effects. Molecular dynamics simulations have also provided insights into the mechanism of the reversal of flap handedness upon binding of a substrate, which varies between closed and semi-open conformations (*25*, *26*).

The effect of drug resistant mutations on the dynamics of the protease has also been studied. Previous, fully atomistic simulations have shown the increase in flexibility of the unliganded form of the drug resistant V82F/I84V double mutant over the wildtype (*27*), with the flaps occupying a semi-open conformation more often in the mutant. Course-grained Brownian dynamics simulations have also shown that an effect of mutations is to reduce the frequency of flap opening with respect to the wildtype thus contributing to a decrease in the association rates of inhibitors (*28*).

However, while significant work has now been done in determining the flap-associated mechanisms of drug-binding to the protease in an open flap conformation, the reverse process of mechanistic drug dissociation remains poorly understood, especially at the atomistic level. Due to the stabilization of the flaps in a closed conformation upon inhibitor binding, the time scale to observe any significant drug deviation away from a bound state coupled to an opening of the flaps has remained beyond the scope of molecular simulation (*21*).

Here, we perform temporally extended, fully atomistic molecular simulations, each of 25 ns with explicit solvent, of the wildtype protease and three drug resistant mutants (G48V, L90M and G48V/L90M) bound to the inhibitor saquinavir. Using several dynamical analyses, including principal component analysis (PCA) (*29*), we provide insights into the first stages of a lateral drug dissociation mechanism from the active site of the protease, following reversion of the flaps into a semi-open conformation. Furthermore, we explore the differential interactions in each protease mutant compared to the wildtype and thus provide insights into the mechanistic basis of drug resistance conferred by the G48V mutation due to enhanced inhibitor coupling with the highly flexible flaps of the protease. Such an expulsion mechanism, which we investigate through the use of steered molecular dynamics simulations (*30*), is not likely to require the full opening of the flaps, and the subsequent alteration of previously proposed dissociation rates for inhibitors from wildtype and mutant proteases (*7*) is therefore discussed.

METHODS

Initial Preparation. The 1HXB crystal structure (resolution 2.3 Å) was used as the starting point for all the molecular dynamics simulations of HIV-1 protease complexed with saquinavir. The residues of protease monomers labeled A and B in the crystal structure were numbered 1−99 and 101−199 respectively. Drug coordinates were extracted and missing hydrogens inserted on the drug using the PRODRG tool (*31*). Gaussian 98 (*32*) was used to perform geometric optimization of the inhibitor at the Hartree Fock level with 6-31G** basis functions. The restrained electrostatic potential (RESP) procedure, which is also part of the AMBER package, was used to calculate the partial atomic charges. The force field parameters for the inhibitor were completely described by the general amber force field (GAFF) (*33*). GAFF has been used before in a comparison between saquinavir and a second generation inhibitor (*10*). Mutations on the protease were incorporated using a protocol from the visualization package VMD (*34*) which also inserted all missing hydrogens on the protease. The standard AMBER force field for bio-organic systems (ff99) (*35*) was used to describe the protein parameters.

A dianionic protonation state was assigned for the aspartic acid dyad. As the protonation state of the aspartic acid dyad can vary under different conditions (see (*36*) and references therein), we also studied the effects of using the alternative, monoprotonated state (see Results and Supporting Information).

The Leap module (*37*) in the AMBER7 software package (*38*) was then used to combine each apo-protease system with the inhibitor. Four Cl^- counterions were added to electrically neutralize each system, which was then solvated using atomistic TIP3P water (*39*) in a cubic box with at least 10 Å distance around the complex. The size of each prepared system was 31845, 31860, 31841 and 31856 atoms for the wildtype G48V, L90M and G48V/L90M systems respectively.

Minimization and Equilibration Protocols. The molecular dynamics package NAMD2 (*40*) was used throughout the production simulations as well as for the employment of minimization and equilibration protocols. Minimization was conducted using the conjugate gradient and line search algorithms available in NAMD2 for 700 iterations for each system with a force constant of 25 kcal/mol/Å ^{2} applied to all restrained atoms. This achieved a desired gradient tolerance of between 10 and 20 in each case. Restrained atoms included all heavy atoms of HIV-1 protease and saquinavir.

The long-range Coulombic interaction was handled using the particle mesh Ewald summation method (PME) (*41*). A nonbonded cutoff distance of 12 Å was used for all simulations. For the equilibration and subsequent production run the SHAKE algorithm (*42*) was employed on all atoms covalently bonded to a hydrogen atom, allowing for an integration time step of 2 fs. Each system was gently annealed from 50 K to 100 K over a period of 10 ps, followed by further annealing to 300 K over a period of 20 ps. The systems were then maintained at a temperature of 300 K using a Langevin thermostat with a coupling coefficient of 5/ps for the rest of the equilibration and for all subsequent production runs. The systems were equilibrated for 200 ps

while maintaining the force constants on the restrained atoms to allow for thorough solvation of the complex and to prevent premature flap collapse (*43*). The L90M and G48V/L90M systems were then equilibrated for 50 ps with the force constraints of all atoms within a 5 Å radius of the L90M mutation and their respective residues set to zero. This was to allow optimal reorientation of the substituted methionine. The atoms within the 5 Å radius of L90M were then kept unrestrained for all further simulations. The force constant on restrained atoms was then reduced sequentially to 20, 15, 10 and 5 kcal/mol/Å ^{2}, equilibrated for 50 ps at each value. This was followed by a completely unrestrained isothermal equilibration for 800 ps in the canonical (NVT) ensemble, and all systems were then simulated for a further 1 ns under NPT conditions using a Berendsen barostat (*44*) with a target pressure of 1 bar and a pressure coupling constant of 0.1 ps.

Production Runs. The output coordinates from each of the four protease systems were then used as the starting point for all subsequent production runs, each of which continued in the NPT ensemble for a further 24 ns. Coordinate trajectories were recorded every 1 ps throughout all equilibration and production runs. In total, over 100 ns of simulation was achieved, performed under conditions of optimal computational efficiency using NAMD2 (*40*), with a wall-clock rate of approximately 8 h/ns, using 30 processors on a 512 processor SGI Altix at CSAR, University of Manchester, U.K., 32 processors (1 node) at the U.K. national HPCx facility, Daresbury, and 32 processors on the TeraGrid cluster at NCSA. These simulations also made use of the U.K. National Grid Service (NGS), specifically 32 processors on the Leeds compte node.

Post-Production Analysis and Steered Molecular Dynamics. Root-mean-squared deviation (RMSD) and distance vector analyses were implemented using VMD. Radii of gyration and radial distribution functions were calculated using the PTRAJ module in the AMBER9 software package. PTRAJ was also used for implementation of principal component analysis (PCA). For PCA, the backbone protease atoms (C_α, C and N) as well as the non-hydrogen drug atoms were used for the analysis. Production trajectories of all systems were combined and fitted to the 1HXB crystal structure; the covariance matrix and principal eigenvectors were calculated using this combined trajectory, making direct comparison between systems possible over a consistent eigenvector set. Principal projections for each system were superimposed every 250 snapshots and represented schematically (see Figure 5) using the IED package (*45*) interfaced with VMD.

Steered molecular dynamics (SMD) simulations were implemented for each protease system using NAMD2, and made use of 32 processors on the Leeds and Oxford compute nodes of the U.K. NGS, from the last coordinates of the unsteered MD simulation. The steered "dummy" atom was attached via a force constant of $k = 10$ kcal/mol/Å ^{2} to all non-hydrogen drug atoms and pulled with a steered velocity of $v = 0.01$ Å/ps. These values of force constant and steered velocity corresponded to a stiff spring in the drift regime (*46*). Furthermore, the velocity was slow enough to allow relaxation of the solvent in response to steering. To prevent translation and rotation of the protease molecule upon application of the steering force, several C_α atoms were held fixed, specifically those of the N- and C-termini residues 1, 99, 100 and 198 as well as residues 30, 108, 123 and 181 at the back end of the protease. The direction of steering was determined by the vector with origin at the C_α atom of residue R108 pointing in the direction of the C_α atom of residue R8; the "dummy" atom was pulled to a distance of 15 Å from its starting position, corresponding to a steered simulation time of 1.5 ns. Center of mass displacement and SMD force values were output every 10 time steps, and all other MD parameters were kept the same as those used in the NPT ensemble, described above.

RESULTS

Structural Flexibility. As a preliminary indication of global backbone flexibility, we measured both the backbone root-mean-squared deviation (RMSD) and the radius of gyration of each of the four systems from their original starting structures across the entire 24 ns trajectory (see Supporting Information). Over the first 5 ns of simulation, no significant difference in RMSD is discernible between any of the systems with values ranging from 1.25 Å to 1.5 Å. However, further RMSD analysis shows that the L90M mutant is more flexible than the other three systems, manifesting the largest deviation from the original structure over the rest of the simulation. There is also little change in the radius of gyration of each of the four systems over such a time scale, with mean values of 17.56 ± 0.37 Å, 17.58 ± 0.37 Å, 17.65 ± 0.39 Å and 17.53 ± 0.39 Å for the wildtype, G48V, L90M and G48V/L90M systems respectively. The results show that the L90M mutant exhibits the largest flexibility in accord with the RMSD analysis.

The backbone root-mean-squared fluctuations (RMSF) relative to the average structure across the whole of the production run for the wildtype, G48V, L90M and G48V/L90M systems are 0.93 ± 0.14 Å, 0.84 ± 0.10 Å, 1.01 ± 0.20 Å and 0.87 ± 0.12 Å respectively, also supporting the slightly increased flexibility of the L90M mutant.

In addition to changes in global flexibility of the enzyme, the specific changes in flexibility across each of the residues were also calculated (see Supporting Information). All systems showed similar fluctuations in their catalytic residues except for monomer B in the L90M mutant system, which showed an RMSF of 1.08 Å as compared to 0.64 Å in the wildtype.

Coupled Flap and Inhibitor Dynamics. Previous studies on HIV apo-proteases have shown that some mutations alter the equilibrium between more open and more closed conformations of the flaps, facilitated by curling of the flap tips (*27*, *47*). Inhibitors have also been shown to stabilize the flaps in a closed conformation (*48*).

To investigate the degree of flap opening in the presence of an inhibitor and the corresponding relationship to the position of the inhibitor, we calculated the evolution of several metrics within the active site (Figure 1(a)). The size of the active site of each protease was measured using the distance between the center of mass of the bottom of the flaps (residues 49 and 149) termed "Flap" and the center of mass of the C_β atoms of the aspartic acid dyad, termed "Asp" (Flap−Asp distance: $|r_{FA}|$). The distances between Flap and the center of mass of saquinavir, termed "Saq" (Flap−Saq distance: $|r_{FS}|$), and between Saq and Asp (Saq−Asp distance: $|r_{SA}|$) were also measured (see Figure 1(b)) as well

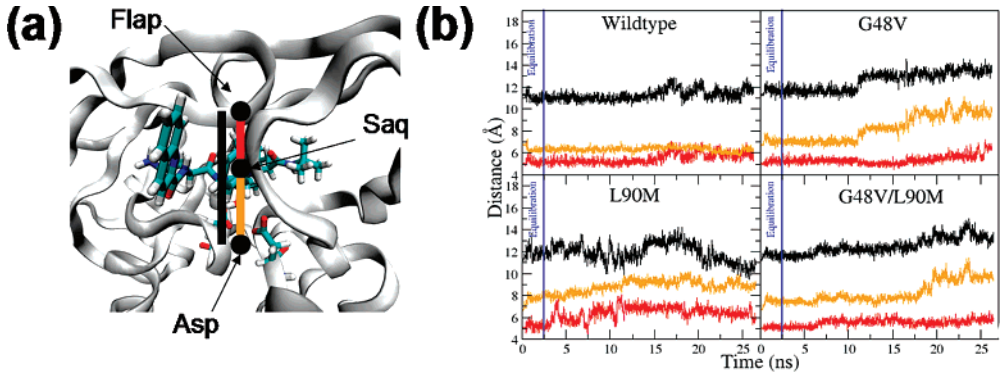

FIGURE 1: (a) Schematic diagram of saquinavir bound to HIV-1 protease. Three coordinates are shown (black circles); Flap, Saq and Asp, defined as the centers of mass of residues 49 of each monomer, all saquinavir atoms, and enzymatic aspartic acid C_β atoms respectively. The black, red and orange lines are the magnitudes of Flap−Asp ($|r_{FA}|$), Flap−Saq ($|r_{FS}|$) and Saq−Asp ($|r_{SA}|$) vectors respectively. (b) Time evolution of the Flap−Asp, Flap−Saq and Saq−Asp vectors over 25 ns for a single representative trajectory of each protease system. Coupled flap−inhibitor motion as well as the transition of the flaps from a closed to a semi-open conformation are observed in the G48V and G48V/L90M systems.

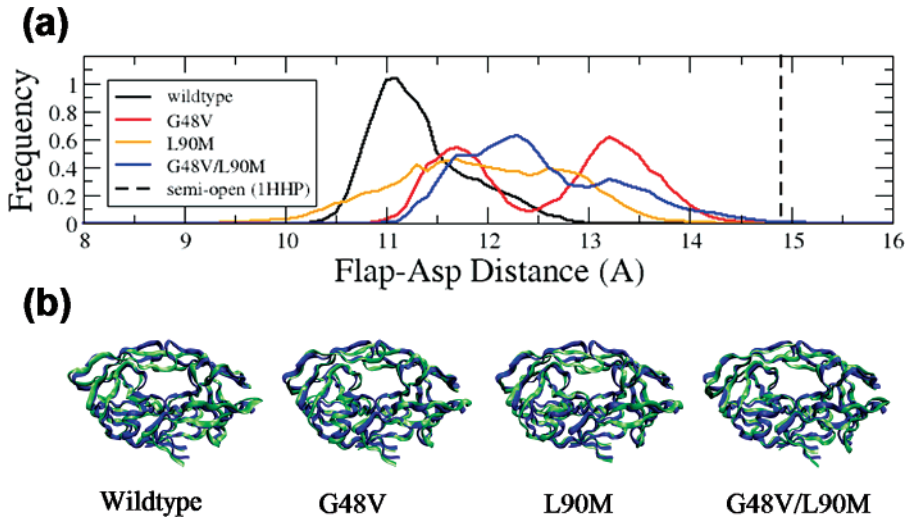

FIGURE 2: (a) Frequency distribution of the Flap−Asp distance for all four systems (wildtype, black; G48V, red; L90M, orange; G48V/L90M, blue). This color coding is used throughout, when all four protease variants are compared to each other. (b) Schematic diagram of the degree of flap opening in each system by the end of the 25 ns simulations (green), as compared to the 1HHP crystal structure (blue). The G48V and G48V/L90M systems sample the most open conformations and reach a semi-open conformation (defined by the 1HHP Flap−Asp distance = 14.9 Å) by the end of the simulation.

as the cross-correlation coefficients (Cc) of these distance metrics across each trajectory (see Supporting Information).

In our simulations, the drug manifests stable binding to the wildtype protease at a distance of 6.5 Å from the aspartic acid dyad, while also stabilizing the flaps at 11 Å. A low cross-correlation coefficient between the Flap−Asp and Saq−Asp distances, $Cc(|r_{FA}|:|r_{SA}|) = 0.41$, indicates that the flap motion is decoupled from the motion of the drug while a high cross-correlation coefficient between the Flap−Asp and Flap−Saq distances, $Cc(|r_{FA}|:|r_{FS}|) = 0.85$, confirms that the drug is coupled tightly to the aspartic acid dyad. Conversely, the G48V mutant shows tight coupling between the motion of the drug and the flaps ($Cc(|r_{FA}|:|r_{SA}|) = 0.91$), demonstrated clearly after 12 ns of simulation, where a discrete change in the Saq−Asp distance (orange line) precedes that of Flap−Asp distance (black line) by approximately 50 ps. In the subsequent 13 ns of the simulation the drug moves nearly 3 Å away from the active site center. The L90M mutant shows the most fluctuation in flap dynamics, although no stable open conformation is achieved by the end of the simulation. Even though there is no significant coupling between the flaps and saquinavir ($Cc(|r_{FA}|:|r_{SA}|) = 0.13$), there is a significant reduction in the coupling between the aspartic acid dyad and the drug ($Cc(|r_{FA}|:|r_{FS}|) = 0.25$), as compared to wildtype. This facilitates significant lateral motion, as indicated by the convergence of the Flap−Asp (black line) and Saq−Asp (orange line) distances. The G48V/L90M double mutant shows stable positioning of the drug in the active site for approximately 19 ns, succeeded by a rapid 3 Å motion away from the aspartic acid dyad within the subsequent 6 ns, during which the drug is clearly coupled to the flaps. This is supported by a high cross-correlation coefficient across the entire trajectory ($Cc(|r_{FA}|:|r_{SA}|) = 0.90$).

The frequency distribution of the Flap−Asp distance for all systems is shown in Figure 2. The PDB structure 1HHP of the apo-protease with flaps in a semi-open conformation was taken as our reference structure. The corresponding Flap−Asp vector for this structure is 14.90 Å. If the conformation of the flaps in the 1HHP structure is taken as a definition of a semi-open conformation, then none of our systems sampled the semi-open conformation significantly, although there were observable differences in the frequency distributions of the Flap−Asp distance exhibited by the

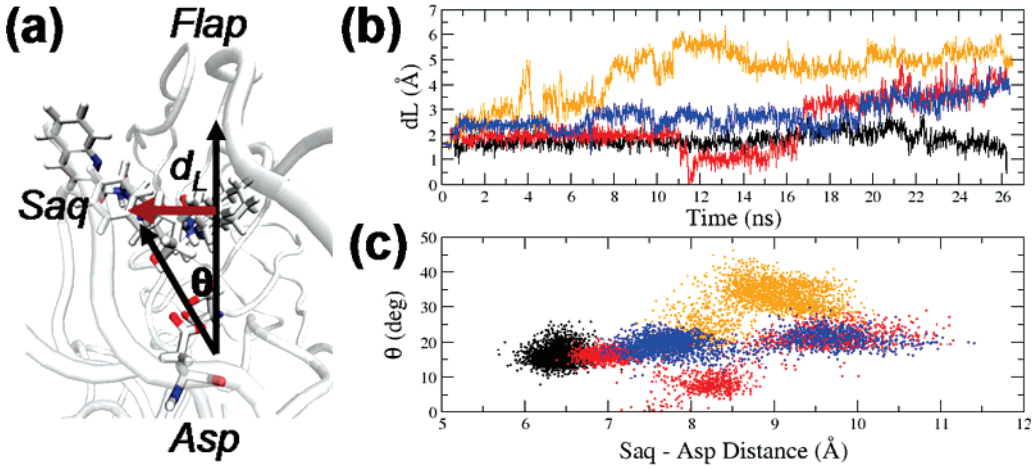

FIGURE 3: (a) Lateral motion of saquinavir out of the active site. The schematic diagram shows the lateral vector d_L measured by the perpendicular distance of the center of mass of saquinavir (Saq) from the Flap−Asp vector (see Figure 1) and the angle θ between the Saq−Asp vector and the Flap−Asp vectors. (b) The time evolution of d_L and (c) the correlation of θ with the magnitude of the Saq−Asp vector.

mutants as compared with the wildtype. While the flaps of the wildtype remained in a closed conformation throughout the 25 ns simulation, the mutants sampled less closed conformations and, in the case of the G48V and G48V/L90M systems, approached the semi-open conformation by the end of the simulation (Figure 2). However, although an interesting bimodal distribution is discernible for the G48V mutant and to a lesser extent for the G48V/L90M mutant, as only one transition of the flaps from a closed to a semi-open conformation is observed in each of these systems, the aforementioned distribution does not represent statistical conformational sampling.

Inhibitor Protrusion and Conformational Changes. Complementary to an analysis of drug motion along the active site axis, angular deviation of the Saq−Asp vector from the Flap−Saq vector together with the perpendicular distance of Saq from the Flap−Asp vector provides a direct indicator of lateral motion (Figure 3). The greatest lateral (d_L) and angular motion (θ) of the drug out of the active site is exhibited by the L90M mutant (orange line), which reaches a distance of 6 Å from the active site only 10 ns into the simulation. G48V (red line) and G48V/L90M (blue line) mutants show trimodal and bimodal distributions respectively, and in both the drug proceeds laterally to a perpendicular distance of 4 Å away from the Flap−Asp vector. Interestingly, in the G48V mutant, the drug first moves into the center of the active site before being laterally directed away from the center. Only in the wildtype (black line) does the drug maintain lateral proximity (perpendicular distance 1 Å to 2.5 Å) to the active site center throughout the simulation.

The protrusion of the quinoline moiety of the P3 subsite (see Figure 4(a)) is observable from the alteration of the radial distribution function of water molecules around it at the end of the simulation as compared to the start. Figure 4(b) shows the radial distribution function of water molecules out to 10 Å from the C35 atom which is the quinoline atom furthest from the central plane of the active site, averaged over 1 ns at the start of the production runs and at the end. The wildtype and L90M systems both show increased exposure to water at the start of the simulation as compared to the end, supporting an increased burying of the quinoline

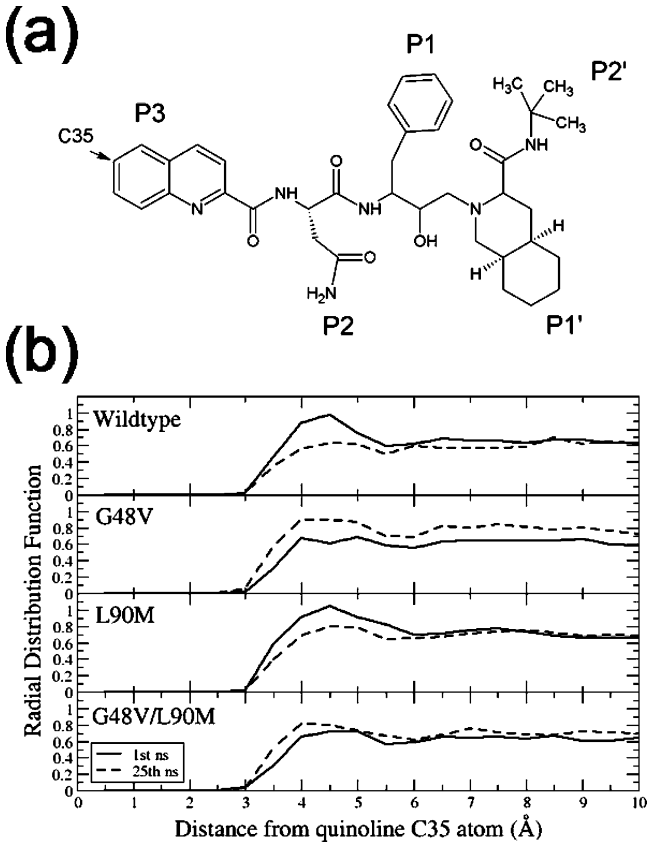

FIGURE 4: (a) Chemical structure of saquinavir showing subsites and the C35 atom on the quinoline moiety. (b) Radial distribution function of water molecules out to 10 Å for all systems for the 1st ns of production (solid line) as compared to the 25th ns (dashed line) of production from the C35 atom. There is increased solvation around the quinoline moiety in the G48V containing systems, associated with a pronounced protrusion from the active site.

moiety into the active site. The G48V and G48V/L90M mutations show converse behavior, in that the quinoline moiety is more exposed to water by the end of the simulation. In fact, for the G48V mutant, the extent of quinoline protrusion is large enough to cause significant increase in the radial distribution function even as far out as 10 Å from the C35 atom.

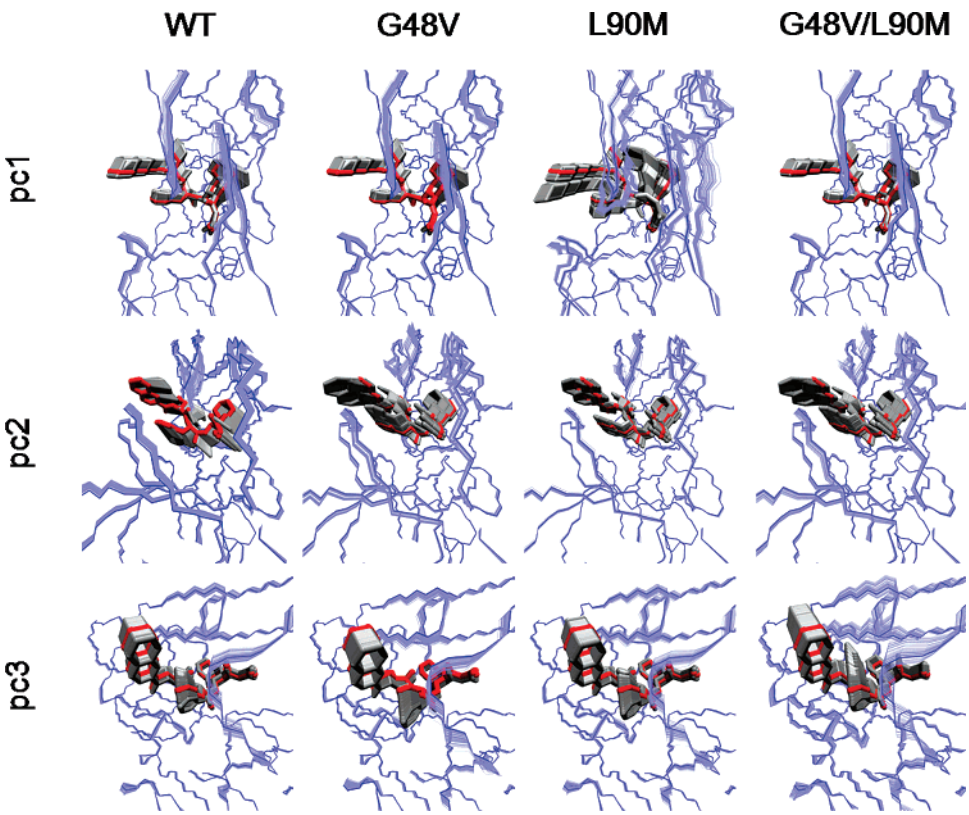

FIGURE 5: Principal component analysis of conformational sampling in each system. Superposition of the projections of each trajectory on the first three common principal component eigenvectors (pc1, pc2 and pc3) for all protease systems. The zero-projection structure is shown in red and blue for the drug and protease respectively, and projections are shown in gray and ice-blue respectively. pc1 is dominated by conformational changes in L90M; the G48V-containing systems exhibit similar conformational sampling in pc2, the drug being laterally displaced from the active site center with pronounced coupling of the drug to the flaps in both pc2 and pc3.

Conformational changes of both the drug and the protease were analyzed further using both RMSD analysis (reported in Supporting Information) and principal component analysis (PCA), reported here. Protease backbone atoms and all non-hydrogen drug atoms were used for PCA, and all production trajectories were combined in order to produce a common set of principal component eigenvectors for all protease systems. The projections of the first three principal components for each system are shown in Figure 5. The zero-projection structures are shown in red and blue for the drug and protease respectively and the corresponding projections onto each principal component, in gray and ice-blue respectively.

As viewed from the top of the flaps looking down, the first principal component eigenvector (pc1) is characterized by the correlated rotations of the drug, such that when the quinoline moiety rotates downward, the P1′ subsite rotates upward into the flaps. This correlates with the up-curling of the flap tips to accommodate the P1′ subsite of the inhibitor. The wildtype, G48V and G48V/L90M systems exhibit similar and only marginal projections onto pc1. The L90M system, however, exhibits two distinct conformational distributions, one similar to that of the other systems and the other corresponding to the large rotational motion described above. This large conformational change is sufficient to dominate the variation across the entire trajectory and results in the motion described uniquely by the L90M system being selected as the first principal component.

The second principal component (pc2) is characterized by the lateral motion of the drug in the active site, correlated with the conformational sampling of the flap of monomer B, as well as the rotation of the phenyl group of the drug in relation to the quinoline moiety. The wildtype uniquely exhibits conformational sampling corresponding to the rotation of the phenyl group down into the active site, as well as sampling of drug conformations closer to the active site center. The L90M projection corresponds to the drug sampling conformations distributed around the zero-projection center, while the G48V-containing systems exhibit projections corresponding to significant lateral motion of the drug out of the active site, as well as the rotation of the phenyl group into a plane parallel to the quinoline moiety. This is coupled to the sampling of more open conformations of the flap of monomer B, which contains a mixture of both lateral and vertical motions.

The third principal component (pc3) is characterized by the conformational flexibility of the flaps as well as the coupled motion of the inhibitor. The flaps in the G48V/L90M system sample significantly more of the conformational space than the wildtype, G48V and L90M systems. The G48V-containing systems exhibit the largest conformational sampling of the drug in relation to conformational changes in the flaps, indicating a more strongly coupled interaction between flaps and inhibitor as compared to the other two systems.

Differential Interactions in the Active Site. In order to investigate the molecular basis for the differential dynamics between the inhibitor and the various protease systems, especially the differential coupling to specific regions of the active site, we analyzed both the hydrophilic and hydrophobic

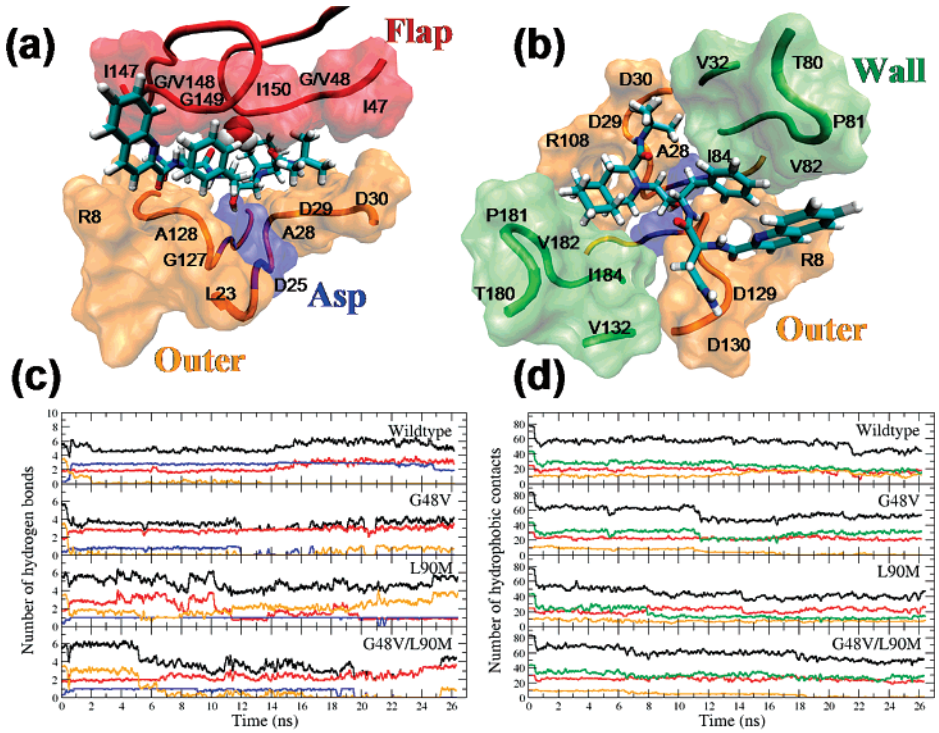

FIGURE 6: Schematic diagrams of active site decomposition into several distinct subregions from (a) side view and (b) top-down view: Flap (residues 47 to 50 and 147 to 150 as well as the tetrahedrally coordinated water molecule between the flaps and the inhibitor), Asp (D25 and D125 residues), Wall (residues V32, P81 to I84, V132 and P181 to I184) and Outer (residues R8, L23, G127 to D130, R108, L123 and G27 to G30). Note also that the flaps are not shown in (b). (c) Time evolution of inhibitor hydrogen bonds with the subregions for each system (note the Wall subregion does not mediate any hydrogen bonds with the drug), using a 100 ps running average window. The wildtype maintains isotropy between the Flap and Asp subregions while in all other systems, Asp hydrogen bonding is significantly reduced and hydrophilic coupling to the flaps is larger. In G48V-containing systems, there is complete loss of Asp hydrogen bonds. (d) Time evolution of hydrophobic contacts with each subregion (note the Asp subregion does not mediate hydrophobic interactions). There is again a distinct loss of inhibitor contact with the Outer subregion in G48V-containing systems. Interactions with all regions are color coordinated, the total interaction being represented by the black line.

interactions within the active site across the course of the simulations.

First, the active site of the protease is decomposed into separate spatial subregions (see Figure 6(a) and 6(b)) in a way that encompasses all hydrophilic and hydrophobic interactions between the drug and the active site. The observed motion of the mutant systems away from the center toward the quinoline moiety "exit" of the active site allows us to define an asymmetric direction to the active site subregions. The components of the active site that are on the P3−P1 side of the drug are therefore referred to as "front" subsites, and those at the other end (P1′ and P2′) are denoted as "back".

The "Flap" subregion consists of residues I47 to I50 (front) and I147 to I150 (back) that make up the inner strands of the flaps as well as the tetrahedrally co-ordinated water molecule between the flaps and the inhibitor. The "Asp" subregion is composed of the catalytic aspartic acid dyad; as it is central in the active site, it is not further designated as "front" or "back". The "Outer" subregion consists of residues G27 to G30, R108 and L123 (back) and G127 to G130, R8 and L23 (front). Finally the "Wall" subregion of the active site consists of V32, P81, V82 and I84 at the front and V132, P181, V182 and I184 at the back. The "Flap" and "Outer" subregions therefore contain a mixture of hydrophilic and hydrophobic residues, while the "Asp" subregion is hydrophilic and the "Wall" subregion entirely hydrophobic. By comparison, the subsites of the drug are largely hydrophobic (P3, P1, P′ and P2′); the only explicitly hydrophilic subsite is P2, identical to an asparagine residue. Other polar groups are largely contained within the backbone of the inhibitor.

Hydrophilic interactions are assessed by calculating the running average number of hydrogen bonds, using a 100 ps time window, between saquinavir and all of the distinct subregions across the simulation span for each system. A donor−acceptor distance of 3.5 Å and a donor−hydrogen−acceptor angle of 150 ° were used as the criteria for the formation of a hydrogen bond (see Figure 6(c)). The total number of hydrogen bonds (black line) throughout the simulations is largest for the wildtype. Furthermore, in the wildtype, there is an isotropic distribution of hydrogen bonds between the "Flap" (red line) and "Asp" (blue line) subregions with running averages of 2.2 and 2.7 bonds respectively as well as almost no hydrogen bonding with the "Outer" (orange line) sub region. The wildtype also exhibits greater hydrogen bonding with the catalytic dyad than any of the mutant systems. This is explained due to the P2 subsite of saquinavir, which bonds uniquely with the dyad in the wildtype, while bonding with the "Flap" subregion in the G48V and L90M systems and, first, with the "Outer" subregion in the G48V/L90M system, later to the "Flap" subregion. Due to this differential coupling in the G48V and G48V/L90M mutants, there is at least one more hydrogen bond with the "Flap" subregion than with the "Asp" for the entire duration of the simulation. The anisotropy is further increased after 12 and 19 ns respectively for these two mutant systems, at which point all hydrogen bonding with the "Asp"

subregion terminates. The increased time to complete decay of hydrogen bonding between the inhibitor and the "Asp" subregion in the G48V mutant is due to the hydroxyethylene group of the inhibitor which switches acceptors from the carbonyl oxygen of D25 to that of D125, hydrogen bonding intermittently for several nanoseconds before being disrupted completely. In both these mutants, there is a decay of hydrogen bonding with the "Outer" subregion within 2 and 6 ns respectively. However, toward the end of the simulations there is re-establishment of a single hydrogen bond between the inhibitor and the highly polar R8 residue.

In the L90M system, there is initially an anisotropic distribution between "Flap" and "Asp" subregions with a 2 hydrogen bond difference, followed by isotropy between all three subregions 11 to 20 ns into the simulation. At this point there is a marked increase in hydrogen bonding by 3 or 4 bonds with the "Outer" subregion. This is due to the hydrogen bond established between the oxygen at the base of the P3 subsite of the drug and the R8 residue as well as the formation of two hydrogen bonds between the P2 subsite and the Outer subregion.

Hydrophobic interactions are assessed by calculating the number of hydrophobic contacts between the drug and the different subregions using the same running average criteria and with the same cutoff distance of 3.5 Å (see Figure 6(c)). The total number of hydrophobic contacts does not vary substantially between the different mutants and the wildtype. However, only in the wildtype is isotropy maintained between all three hydrophobic subregions. The significant number of contacts with the "Wall" subregion is maintained owing to the proximity of the P1, P1′ and P2′ subsites, while contact with the "Flap" subregion is mediated by a combination of all the hydrophobic subsites. Interestingly, unlike the hydrophilic interaction in the wildtype, which decays to zero, there is a pronounced hydrophobic interaction with the "Outer" subregion, owing again to the P1′ and P2′ subsites. At 15 ns into the wildtype simulation there is complete convergence between the number of "Flap" and "Outer" contacts due to a conformational change in the P1 subsite toward L23. This again is unique to the wildtype; in all mutant systems, the P1 subsite remains coupled to the "Flap" subregion. In the G48V and G48V/L90M systems, there is a decay in the number of contacts with the "Outer" subregion at 12 and 19 ns which again coincides with the previously mentioned rise in the position of the drug with respect to the base of the active site and the protrusion of the inhibitor. Finally there is an inversion in the number of contacts with the "Flap" and "Wall" subregions in the L90M system, owing to a conformational change in the P1′ subsite by which it associates with the "Flap" subregion instead of the "Wall".

The running average number of water molecules within 3 Å around the catalytic dyad was calculated across the entire trajectory for each system (see Supporting Information), again with a time window of 100 ps. In all mutants there are at least two water molecules coordinated around the catalytic dyad within 5 ns of the beginning of the simulation. In contrast, the wildtype protease exhibits no water coordination around the dyad until after 20 ns of simulation. The difference in water coordination between the wildtype and mutant systems ranges from 0 to 8, and by the end of the simulation there is still a coordination difference of 2 between wildtype and mutant systems. The previously mentioned abrupt changes in the Flap−Asp and Saq−Asp vectors for both the G48V and G48V/L90M systems after 12 and 19 ns respectively, as well as termination of hydrogen bonds with the "Asp" subregion, coincide with increased water coordination around the catalytic dyad. In particular, at these points a water molecule enters into the cavity between the dianionic dyad and the hydroxyethylene group of saquinavir, in both systems leading to disruption of the hydrogen bond between the dyad and the inhibitor. For the wildtype and L90M systems, even though increased water coordination occurs, direct hydrogen bonding between the inhibitor and the dyad is not disrupted by any specific water molecule.

Mutation-Assisted Lateral Inhibitor Escape. To understand the molecular mechanism for the first stages of translation out of the active site, observed in all three mutants, and to assess the subsequent ease of lateral escape, we further investigated the change in the subsite interaction properties of the drug with various active site subregions across the course of the simulations, as well as laterally extracting the drug from the ative site through steered molecular dynamics (SMD) simulations from the final conformation attained by the drug in each system.

In the L90M mutant, a clear mechanism for drug translation was not discernible. The cause of the observed lateral displacement of the center of mass (see Figure 3) is the increased flexibility of the mutant protease as well as increased hydrophobic association of the P1′ subsite with the flaps through a conformational change, which places the subsite in between the I50 and I150 residues of the protease. Furthermore, the protrusion signature of the quinoline moiety as calculated by the radial distribution function (see Figure 4) is less at the end than at the start of the simulation in the L90M mutant: no clear mechanism of translation was observed over the course of the simulation.

By contrast, the drug in both the G48V and G48V/L90M mutant proteases not only shows substantial deviation from the original position but also shares a common mechanism of translation. The properties of increased flap coupling, combined with a loss of hydrophobic contacts and hydrogen bonds with the "Outer" subregion, are common to both G48V containing mutants (see Figure 6(c) and 6(d)), as well as a similar signature of quinoline protrusion from the active site (Figure 4).

Figure 7 shows key drug−protease interactions in the G48V system at the start (Figures 7(a) and 7(b)) and the end (Figures 7(c) and 7(d)) of the simulation. At the start of the simulation, the P1′ and P2′ subsites form hydrophobic contacts with the back part of the "Outer" subregion (specifically with residues L23 and A28 respectively). These contacts are lost at 12 and 17 ns respectively (Figures 7(e)-[1] and 7(e)[2]) and are correlated with an increase in hydrophobic contacts with the Flap and Wall subregions. This is due to a translation of the P1′ subsite away from L23 and a rotation of the P2′ subsite into the hydrophobic Wall cavity composed of V32, P81, V82 and I84 residues (Figure 7(c)). Furthermore, unlike the wildtype system in which the P1 subsite rotates to form hydrophobic contacts with the front "Outer" subregion, the presence of valine at position 148 allows maintenance of hydrophobic contacts with the flaps in the G48V containing mutants. This results in the P1 subsite, which initially also has hydrophobic contacts with the Wall cavity, moving clear of it by the end of the

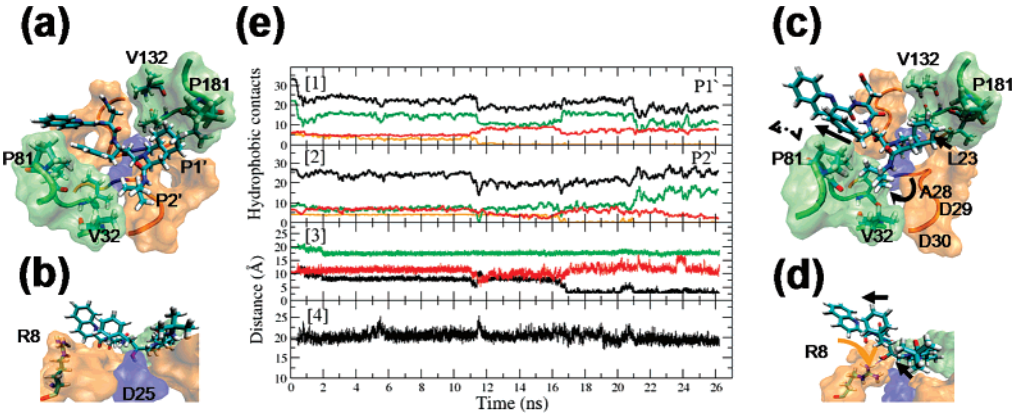

FIGURE 7: (a) Distinct inhibitor subsite contacts with active site subregions and (b) position of the R8 "gate" residue for the G48V mutant system at the start of the simulation. (c) Unidirectional translation of P1, P1′ and P2′ inhibitor subsites in the G48V system and (d) position of inward rotated R8 "gate" residue at the end of the simulation. (e) Time evolution of hydrophobic contacts of [1] the P1′ and [2] the P2′ subsites with the active site subregions, following the same color scheme as Figure 6. Complete decay of contacts with the back Outer subregion occurs as well as transfer of subsite contacts to the Flap and Wall subregions. [3] Interatomic distances for R8 and R108 C_α atoms (green line), saquinavir hydroxythylene group oxygen SAQ:O−R8:NH1 atom (black line) and SAQ:O−R108:NH1 (red line). While interatomic separation of the backbone of R8 and R108 gate residues remains constant, a combination of inhibitor motion toward R8 and away from R108 as well as rotation of R8 toward the hydroxythylene oxygen results in the formation of a hydrogen bond. [4] Time evolution of the interatomic separation of P81 and P181 C_α Wall tip residues. The Wall tip breathes with distance fluctuations up to 5 Å, allowing for the passage of the P1 subsite past the Wall region in the course of the simulation.

simulation. This is facilitated by the flexibility of the Wall tip, the Wall tip distance (P81−P181 C_α) varying by up to 5 Å across the simulation (Figure 7(e)[4]); such breathing allows the P1 subsite to move beyond the hydrophobic pocket initially constraining it.

As well as conformational changes in the drug, we noticed a large conformational change in the R8 residue which guards the exit to the active site (Figure 7(b) and (d)). At the beginning of the simulation, both "gate" arginines R8 and R108 are approximately equidistant to the hydroxyethylene moiety of the inhibitor. Figure 7(e)[3] shows the evolution of these distances over the course of the simulation. At 17 ns into the simulation, there is a coupled movement of the OH group away from R108 (red line) and toward R8 (black line), as well as significant motion of R8 toward the OH group. This coincides with the loss of hydrogen bonding with the aspartic acid dyad (Figure 6(e)), following the flap-induced lifting of the drug at 17 ns (Figure 1 orange line).

The R8 conformational change establishes a stable, strong hydrogen bond which endures for the remainder of the simulation, preventing motion of the OH group back toward the catalytic dyad and subsequent re-formation of a hydrogen bond with it. Stability of the arginine backbone is confirmed by the constancy of the inter-arginine C_α separation (green line) and confirms a rotation of R8 toward the drug (Figure 7(e)) instead of motion of the backbone. All of these mechanisms also occur in the G48V/L90M mutant (data not shown), but do not appear in either the L90M or the wildtype systems.

SMD simulations of lateral drug extraction from the active site reveal that the G48V-containing systems share a similar force profile to the wildtype but with varying magnitude (see Figure 8). The wildtype exhibits a well-defined two-phase extraction profile; the resistive force of the first barrier (∼1000 pN) occurs at around 500 ps into the extraction and is due to the conformation adopted by the R8 residue (see Figure 7(d)), which obstructs the P1 subsite as well as the P1′ and P2′ subsites being pulled underneath the flaps. The second barrier (∼750 pN) is due to the hydrophobic interactions mediated by the P1′ and P2′ subsites as they are pulled completely clear of the flaps of the protease approximately 1000 ps into the simulation.

The G48V-containing systems also exhibit a two-phase extraction profile with a significantly reduced peak resistive force upon extraction (∼600 pN) as compared to the wildtype system. This occurs at around 440 and 600 ps into the simulation for the G48V and G48V/L90M systems respectively. The coupled motion of the drug toward the flaps and the R8 conformation adopted by the G48V-containing systems in the conventional MD simulations (see Figure 7(d)) allow the P1 subsite to be already clear of the R8 residue, thus avoiding any additional barriers caused by lateral obstruction of R8 and explaining the reduced force exhibited by the G48V-containing systems. Furthermore, as the drug is already more laterally displaced in the G48V-containing mutants at the start of the SMD simulations, the P1′ and P2′ subsites do not interact as much with the "back" flap. The main barrier to overcome is that of the P1′ and P2′ subsites moving past the front flap. The small secondary force peaks of ∼400 pN and ∼350 pN exhibited in these systems at around 900 and 1000 ps respectively into the simulations are due to residual interactions of the P2′ subsite with the front "Wall" of the protease.

The L90M mutant exhibits a substantially different extraction profile from the other three systems with a resistive force fluctuating around 500 pN for the whole simulation. This is due to the P1′ and P2′ subsites being caught between the flaps of the protease. Upon extraction the hydrophobic interactions between the front flap and the P1′ and P2′ subsites are maintained and the flap rotates laterally outward as the drug is expelled.

Previous molecular simulations on the protease complexed with saquinavir have suggested a monoprotonated dyad with Asp 25 being thermodynamically favored (*49*). However, at physiological pH the catalytic dyad is dianionic, and so the proton would have to bind after or upon ligand binding. We, therefore, also investigated the effects of altering the protonation state of the catalytic dyad. A full account can be

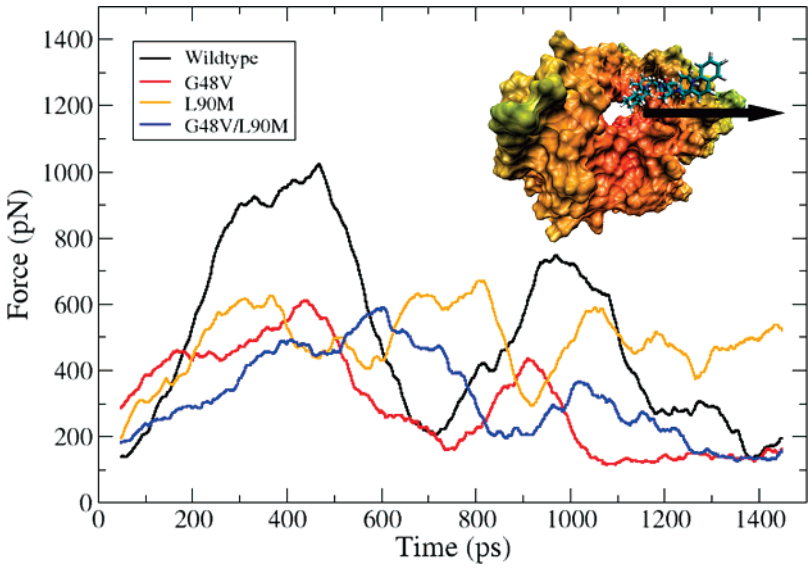

FIGURE 8: Steered molecular dynamics (SMD) lateral extraction of saquinavir from the HIV-1 protease active site. The force is calculated using a running average time window of 100 ps. The wildtype exhibits a well-defined two-phase extraction profile, the first barrier being due to the conformation adopted by the R8 residue (see Figure 7(d)), which obstructs the P1 subsite during drug extraction. The second is due to the hydrophobic interactions mediated by the P1′ and P2′ subsites as they are pulled past the flaps of the protease. The G48V-containing mutants are initially already more laterally displaced than the wildtype. The resistive force along the steered pathway is subsequently smaller for the G48V-containing systems as compared to the wildtype by approximately 400 pN.

found in the Supporting Information, but we also provide a brief summary of the results here.

Simulation of all four protease systems over a period of 10 ns, with the dyad in a monoprotonated state, reveals the comparative immobility of the drug and the flaps of the protease in these systems. The flaps remain in a closed conformation with a Flap−Asp distance of around 12 Å, while the drug shows no flap-coupling in any system, nor does it exhibit significant lateral motion out of the active site. Indeed, lateral motion is largest for the wildtype system, for which the center of mass of the drug moves approximately only 1 Å from the starting position. The first stage of the G48V-assisted escape mechanism, reported here, is therefore facilitated more by a dianionic dyad state than a monoprotonated state and is thus able to take advantage of the dianionic state to confer drug resistance.

DISCUSSION

In order to provide molecular insight into the kinetic basis of drug resistance conferred by the characteristic G48V and L90M mutations of HIV-1 protease to the inhibitor saquinavir, we have compared the dynamics of the two single mutants and the G48V/L90M double mutant bound to the drug, over 25 ns molecular dynamics simulations in explicit water. Our results show that the degree of isotropy of hydrogen bonding and hydrophobic contacts, between the inhibitor and various subregions of the active site, plays a key role in determining the subsequent dynamics of the inhibitor. Only in the wildtype is there a significant isotropic distribution between flap−inhibitor and catalytic dyad−inhibitor hydrogen bonds (Figure 6(c)), due to drug P2 subsite bonding with the dyad as well as isotropy in the hydrophobic contacts with different subregions of the active site (Figure 6(d)). Consequently, there is little bulk motion of the inhibitor within the active site across the entire 25 ns, as well as no change in the conformation of the flaps (Figures 1, 2).

We observe a common mechanism of drug translation out of the active site in the G48V-containing mutants over the 25 ns period. The presence of the G48V mutation in the protease not only increases hydrophobic interactions with the P3 and P1 subsites, but induces an extra hydrogen bond between the P2 subsite and the flaps. This, together with the lack of significant hydrogen bonds with the catalytic dyad for these mutants, has a pronounced effect (Figure 6).

First, increased flap coupling facilitates motion of the inhibitor toward the flaps (Figure 1), leading to complete disruption of hydrogen bonding with the catalytic dyad (Figure 6) as well as coinciding with entry of water molecules into the catalytic region (see Supporting Information). Second, it induces the flaps to sample more open conformations, in turn leading to further subsequent motion of the inhibitor away from the catalytic dyad.

Flap induced lifting of the drug away from the dyad also causes loss of hydrophobic interactions between the P1′ and P2′ subsites with L23 and A28 hydrophobic residues in the outer regions of the active site, resulting in the pronounced rotation of P2′ respectively into the Wall subregion cavity composed of V32, P81, V82 and I84 (Figure 7). The P1 subsite moves clear of this hydrophobic well, facilitated by significant breathing of the Wall tip residues, and the quinoline moiety of the drug becomes more exposed to solvent (Figure 4) due to a 4 Å lateral shift out of the active site (Figure 3). Furthermore, principal component analysis (PCA) confirms the significant increase in lateral conformational sampling by the drug in the G48V-containing mutants (see Figure 5(pc2)) as well as the coupled expulsive motion of the flaps. Such lateral drug translation induces a conformational change in the R8 active site gate residue, which subsequently forms a hydrogen bond with the emerging central hydroxyethylene moiety of the drug (Figure 7).

Although, by the end of these simulations, the drug has not been completely expelled from the active site, the

distinctive mechanisms described above, together with their occurrence in both G48V-containing mutants, provide compelling insight into a plausible mechanism of lateral drug escape from the active site. By the end of the simulations, the flaps in these mutants are in a semi-open conformation; the only remaining steric barrier to complete drug expulsion is the Wall tip residue P81 constraining the P2′ subsite. However, the breathing capability of this tip implies that, over a longer time scale, such a steric barrier would diminish, allowing for complete expulsion to occur. SMD simulations of the drug in the direction of lateral extraction (see Figure 8) confirm the relative ease with which the G48V-containing mutants can be extracted in comparison to the wildtype and are comparable with steered dissociation forces observed in studies of different biomolecular systems (*50*).

The increased sampling of more semi-open conformations of the flaps in the mutant proteases, especially the G48V and G48V/L90M systems, agrees well with previous computational studies on apo-proteases (*27*) over a similar time scale. In those studies the extent of flap opening was marginally greater than in our studies owing to the absence of a bound inhibitor. Previous studies on the multi-nanosecond time scale have also shown that the flaps are stabilized in a closed position when bound to an inhibitor (*21*). However, in those simulations, an implicit solvent was used, resulting in decreased solvent viscosity. This results in enhanced flap opening in the apo-protease while the reverse effect is expected in the inhibitor bound case due to the increased apparent strength of flap−inhibitor interactions.

In our simulations, using explicit solvent, we show a transition to the semi-open conformation while the inhibitor is bound to the protease. The fact that G48V-containing systems reach a semi-open conformation by the end of the 25 ns simulation, in the presence of an inhibitor, is consistent both with an increase in sampling of semi-open conformations by mutant proteases and with a slightly reduced rate of opening of the flaps in an inhibitor-bound protease as compared to an apo-protease.

Furthermore, the significant deviation of the inhibitor away from the initial position reported here and the relative ease of extraction using SMD, together with the fact that full flap opening is rare compared to the semi-open conformation (*21*), provide a strong basis for the hypothesis that lateral drug expulsion from a semi-open protease is possible.

Binding of peptidomimetic inhibitors to the protease occurs by a previously cited two step process (*16*):

$$\mathrm{E_o} + \mathrm{I} \underset{k_{-1}}{\overset{k_1}{\rightleftharpoons}} \mathrm{E_o{\cdot}I} \underset{k_{-2}}{\overset{k_2}{\rightleftharpoons}} \mathrm{E_c{\cdot}I} \qquad (1)$$

where I represents the inhibitor, E_o·I and E_c·I represent "loose" and "tight" forms of the protease complex with the flaps in an "open" and "closed" form respectively and k_1, $k_{-1}$and k_2, k_{-2} are the rate constants from the first and second steps of these complexes respectively. In such a process, the combination of the forward and backward rates give rise to observable association (k_{on}) and dissociation (k_{off}) rate constants from unbound to tightly bound proteases. It has recently been shown, using coarse-grained Brownian dynamics simulations, that binding of ligands is gated by the flaps, which modulate access to the active site (*28*). Gating rates for the G48V and L90M mutations alone were comparable to the wildtype in these studies, while being smaller for proteases with several mutations including these two mutations. In the above context, changes in "slow gating" observed in these studies correspond to alteration in k_1.

Previous authors attributed the decrease in binding affinity of saquinavir with mutant proteases, represented by an increase in k_{off}, to a decrease in the equilibrium constant ($K_E = k_2/k_{-2}$) between "tight" and "loose" forms of the complex (*7*). Furthermore, complete dissociation of the inhibitor from the protease was only suggested from the flap-open protease.

Based on our simulations, which exhibit a tendency toward lateral expulsion, we propose a simultaneously occurring and alternative mechanism for the increase in k_{off} induced by the G48V mutant, which results in a decrease in the dissociation constant. In such a mechanism, complete dissociation can occur with the protease in a semi-open flap conformation:

$$E_{so} + \mathrm{I} \underset{k_{-3}}{\overset{k_3}{\rightleftharpoons}} \mathrm{E_{so}{\cdot}I} \underset{k_{-4}}{\overset{k_4}{\rightleftharpoons}} \mathrm{E_c{\cdot}I} \qquad (2)$$

E_{so} represents the unbound form of the enzyme with the flaps in a semi-open conformation. The rate constants k_3 and k_{-3} are for binding and unbinding of inhibitors from a semi-open apo-protease.

As binding of inhibitors is most likely diffusion limited (*28*), it is plausible that k_3 is sufficiently small as not to be an alternative viable mechanism for binding, thus preserving the original two-step binding process. From the bound state however, inhibitor dissociation may proceed via both mechanisms provided k_{-3} is not too small. Furthermore, as experimentally k_{on} is found not to change significantly in the G48V mutant, resistance may be manifested by an increase in k_{-3} as compared to the wildtype, as well as the increase in k_{-2} suggested by previous authors (*7*). This slight increase would mean that it is additionally viable for the inhibitor to become unbound via a lateral expulsion mechanism before being restabilized in a flap-closed protease. In the case of the G48V mutant systems simulated here, it is the increased coupling of the flaps to the inhibitor that alters the position of the drug sufficiently explaining how k_{-3} could be increased while, even though some flap fluctuation is observed in the wildtype (Figure 1), the lack of extensive coupling prevents the drug from any large slip in positioning. Furthermore, it is plausible that there may be a whole class of mutations for various inhibitors that takes advantage of the increased rate of such lateral inhibitor expulsion to confer resistance to inhibitor binding. It would be very interesting to see the effects of such long time scale simulations on different inhibitor/mutant combinations.

Our study shows that the dianionic protonation state of the catalytic dyad plays a significant part in the assistance of the observed lateral motion. A mechanism of lateral dissociation in alternative protonation states has not been reported in the literature, nor in our own studies of the protease in the monoprotonated state, in which no lateral motion is observed over a time scale of 10 ns (see Results and Supporting Information). As any protonation of the dyad most likely occurs upon or after ligand binding (*36*), our work shows that the G48V mutation is able to take advantage of the dianionic state of the protease to confer drug resistance through the expulsion mechanism described here.

Finally, the significant translation of the inhibitor in a concerted direction provides the basis for an improved strategy in drug design. Steric hindrance of the large P3 subsite/quinoline moiety with the flaps prevents lateral shift of the inhibitor toward the P1′ and P2′ side exit of the active site in the semi-open conformation, thus acting as an "anchor". The lack of a sufficiently large anchor at the other end of the drug, especially one that can oppose lateral motion through steric hindrance with the flaps, allows the drug to be translated unidirectionally. Inhibitors with symmetric and sufficiently sized anchors at both ends of the drug may enhance drug binding in the semi-open state and counter the translational effects induced by excessive flap coupling. Indeed, the lack of sufficient interaction with the catalytic dyad in the mutants studied here promotes this excessive flap coupling. Inhibitors should therefore also be designed to incorporate stronger binding with the catalytic dyad.

ACKNOWLEDGMENT

We thank Professor David Wild for initial discussions which led to this project and Dr. Simon Clifford for helpful discussions regarding *ab initio* methods.

SUPPORTING INFORMATION AVAILABLE

Graphical analysis of the global structural flexibility of the enzyme backbone is provided as well as changes in flexibility across amino acid residues. There are also additional specifications of cross-correlation coefficients between drug and protease distance vectors and supplemental RMSD analysis of net drug-conformational changes. Graphical analysis of the water-coordination around the dyad is also provided. Finally, there is a full account of the molecular dynamics of saquinavir bound to HIV-1 protease variants in the monoprotonated dyadic state. This material is available free of charge via the Internet at http://pubs.acs.org.

REFERENCES

1. Wlodawer, A., and Erickson, J. W. (1993) Structure-based inhibitors of HIV-1 protease, *Annu. Rev. Biochem. 62*, 543−585.
2. Wlodawer, A., and Vondrasek, J. (1998) Inhibitors of HIV-1 Protease: A Major Success of Structure-Assissted Drug Design, *Annu. Rev. Biophys. Biomol. Struct. 27*, 249−284.
3. Hoffman, N. G., Schiffer, C. A., and Swanstrom, R. (2003) Covariation of amino acid positions in HIV-1 protease, *Virology 314*, 536−548.
4. Svicher, V., Ceccherini-Silberstein, F., Erba, F., Santoro, M., Gori, C., Bellochi, M. C., Giannella, S., Trotta, M. P., d'Arminio Monforte, A., Antinori, A., and Perno, C. F. (2005) Novel human immunodeficiency virus type 1 protease mutations potentially involved in resistance to protease inhibitors, *Antimicrob. Agents Chemother. 49*, 2015−2025.
5. Wu, T. D., Schiffer, C. A., Gonzales, M., Taylor, J., Kantor, R., Chou, S., Israelski, D., Zolopa, A. R., Fessel, W. J., and Shafer, R. W. (2003) Mutation Patterns and Structural Correlates in Human Immunodeficiency Virus Type 1 Protease following Different Protease Inhibitor Treatments, *J. Virol. 77*, 4836−4847.
6. Yahi, N., Tamalet, C., Tourres, C., Tivoli, N., Ariasi, F., Volot, F., Gastaut, J.-A., Gallais, H., Moreau, J., and Fantini, J. (1999) Mutation patterns of the reverse transcriptase and protease genes in human immunodeficiency virus type 1-infected patients undergoing combination therapy: Survey of 787 sequences, *J. Clin. Microbiol. 37*, 4099−4106.
7. Maschera, B., Darby, G., Palu, G., Wright, L. L., Tisdale, M., Myers, R., Blair, E. D., and Furfine, E. S. (1996) Human Immunodeficiency Virus: Mutations in the viral protease that confer resistance to saquinavir increase the dissociation rate constant of the protease-saquinavir complex, *J. Biol. Chem. 271*, 33231−33235.
8. Ohtaka, H., Schon, A., and Freire, E. (2003) Multidrug resistance to hiv-1 protease inhibition requires cooperative coupling between distal mutations, *Biochemistry 42*, 13659−13666.
9. Todd, M. J., Luque, I., Velazquez-Campoy, A., and Freire, E. (2000) Thermodynamic Basis of Resistance to HIV-1 Protease Inhibition: Calorimetric Analysis of the V82F/I84V Active Site Resistant Mutant, *Biochemistry 39*, 11876−11883.
10. Lepsik, M., Kriz, Z., and Havlas, Z. (2004) Efficiency of a Second-Generation HIV-1 Protease Inhibitor Studied by Molecular Dynamics and Absolute Binding Free Energy Calculations, *Proteins: Struct. Funct. Bioinf. 57*, 279−293.
11. Wang, W., and Kollman, P. A. (2001) Computational study of protein specificity: The molecular basis of HIV-1 protease drug resistance, *Proc. Natl. Acad. Sci. U.S.A. 98*, 14937−14942.
12. Zoete, V., Michielin, O., and Karplus, M. (2003) Protein-ligand binding free energy estimation using molecular mechanics and continuum electrostatics. application to hiv-1 protease inhibitors, *J. Comput.-Aided Mol. Des. 17*, 861−880.
13. Collins, J. R., Burt, S. K., and Erickson, J. W. (1995) Flap opening in HIV-1 protease simulated by 'activated' molecular dynamics, *Nat. Struct. Biol. 2*, 334−338.
14. Piana, S., Carloni, P., and Rothlisberger, U. (2002) Drug resistance in HIV-1 protease: Flexibility-assisted mechanism of compensatory mutations, *Protein Sci. 11*, 2393−2402.
15. Johnson, V. A., Brun-Vezinet, F., Clotet, B., Conway, B., Kuritzkes, D. R., Pillay, D., Schapiro, J., Telenti, A., and Richman, D. (2005) Update of the Drug Resistance Mutations in HIV-1: 2005, *Int. AIDS Soc.—U.S.A. 13*, 51−57.
16. Furfine, E. S., D'Souza, E., Ingold, K. J., Leban, J. J., Spector, T., and Porter, D. J. T. (1992) Two-step binding mechanism for HIV protease inhibitors, *Biochemistry 31*, 7886−7891.
17. Zoete, V., Michielin, O., and Karplus, M. (2002) Relation between Sequence and Structure of HIV-1 Protease Inhibitor Complexes: A Model System for the Analysis of Protein Flexibility, *J. Mol. Biol. 315*, 21−52.
18. Kumar, M., and Hosur, M. V. (2003) Adaptability and flexibility of HIV-1 protease, *Eur. J. Biochem. 270*, 1231−1239.
19. Scott, W. R. P., and Schiffer, C. A. (2000) Curling of Flap Tips in HIV-1 Protease as a Mechanism for Substrate Entry and Tolerance of Drug Resistance, *Structure 8*, 1259−1265.
20. Wang, W., and Kollman, P. A. (2000) Free energy calculations on dimer stability of the hiv protease using molecular dynamics and a continuum solvent model, *J. Mol. Biol. 303*, 567−582.
21. Hornak, V., Okur, A., Rizzo, R. C., and Simmerling, C. (2006b) HIV-1 protease flaps spontaneously open and reclose in molecular dynamics simulations, *Proc. Natl. Acad. Sci. U.S.A. 103*, 915−920.
22. Freedberg, D. I., Ishima, R., Jacob, J., Wang, Y.-X., Kustanovich, I., Louis, J. M., and Torchia, D. A. (2002) Rapid structural fluctuations of the free HIV protease flaps in solution: Relationship to crystal structures and comparison with predictions of dynamics calculations, *Protein Sci. 11*, 221−232.
23. Ishima, R., Freedberg, D. I., Wang, Y. X., Louis, J. M., and Torchia, D. A. (1999) Flap opening and dimer-interface flexibility in the free and inhibitor-bound HIV protease, and their implications for function, *Struct. Fold. Des. 7*, 1047−1055.
24. Rose, J. R., Babe, L. M., and Craik, C. S. (2006) The Open Structure of a Multi-Drug-Resistant HIV-1 Protease is Stabilized by Crystal Packing Contacts, *J. Am. Chem. Soc. 128*, 13360−13361.
25. Toth, G., and Borics, A. (2006a) Closing of the Flaps of HIV-1 Protease Induced by Substrate Binding: A Model of a Flap Closing Mechanism in Retroviral Aspartic Proteases, *Biochemistry 45*, 6606−6614.
26. Toth, G., and Borics, A. (2006b) Flap opening mechanism of HIV-1 protease, *J. Mol. Graphics Modell. 24*, 465−474.
27. Perryman, A. L., Lin, J., and McCammon, J. A. (2004) HIV-1 protease molecular dynamics of a wild-type and of the V82F/I84V mutant: Possible contributions to drug resistance and a potential new target site for drugs, *Protein Sci. 13*, 1108−1123.
28. Chang, C.-E., Shen, T., Trylska, J., Tozzini, V., and McCammon, J. A. (2006) Gated binding of ligands to HIV-1 protease: Brownian dynamics simulations in a coarse-grained model, *Biophys. J. 90*, 3880−3885.
29. Balsera, M. A., Wriggers, W., Oono, Y., and Schulten, K. (1996) Principal component analysis and long time protein dynamics, *J. Phys. Chem. 100*, 2567−2572.

30. Isralewitz, B., Gao, M., and Schulten, K. (2001) Steered molecular dynamics and mechanical functions of proteins, *Curr. Opin. Struct. Biol. 11*, 224−230.
31. Schuettelkopf, A. W., and van Aalten, D. M. F. (2004) PRODRG - a tool for high-throughput crystallography of protein-ligand complexes, *Acta Crystallogr. D60*, 1355−1363.
32. Frisch, M. J., Trucks, G. W., Schlegel, H. B., Scuseria, G. E., Robe, M. A., Cheeseman, J. R., Zakrzewski, V. G., Montgomery, J. A., Stratman, J., Burant, J. C., et al. (2002) *Gaussian 98*, Gaussian Inc., Pittsburgh, PA
33. Wang, J., Wolf, R. M., Case, D. A., and Kollman, P. A. (2004) Development and Testing of a General AMBER Force Field (GAFF), *J. Comput. Chem. 25*, 1157−1174.
34. Humphrey, W., Dalke, A., and Schulten, K. (1996) VMD−Visual Molecular Dynamics, *J. Mol. Graphics 14*, 33−38.
35. Wang, J. M., Cieplak, P., and Kollman, P. A. (2000) How well does a restrained electrostatic potential (RESP) model perform in calculating conformational energies of organic and biological molecules, *J. Comput. Chem. 21*, 1049−1074.
36. Kovalskyy, D., Dubyna, V., Mark, A. E., and Korenelyuk, A. (2005) A molecular dynamics study of the structural stability of HIV-1 protease under physiological conditions: The role of Na+ ions in stabilizing the active site, *Proteins: Struct. Funct. Bioinf. 58*, 450−458.
37. Schafmeister, C. E. A. F., Ross, W. S., and Romanovski, V. (1995) *LEaP*, University of California, San Francisco, CA.
38. Case, D. A., Pearlman, J. C. D. III. T. C., Wang, J., Ross, W., Simmerling, C., Darden, T., Merz, T., Stanton, R., Cheng, A., et al. (2002) *AMBER7*, University of California, San Francisco, CA.
39. Jorgensen, W. L., Chandrasekhar, J., Madura, J. D., Impey, R. W., and Klein, M. L. (1983) Comparison of simple potential functions for simulating liquid water, *J. Chem. Phys. 79*, 926−935.
40. Kale, L., Skeel, R., Bhandarkar, M., Brunner, R., Gursoy, A., Krawetz, N., Phillips, J., Shinozaki, A., Varadarajan, K., and Schulten, K. (1999) NAMD2: Greater scalability for parallel molecular dynamics, *J. Comput. Phys. 151*, 283−312.
41. Essmann, U., Perera, L., Berkowitz, M. L., and Darden, T. (1995) A smooth particle mesh Ewald method, *J. Chem. Phys. 103*, 8577−9593.
42. Ryckaert, J. P., Ciccotti, G., and Berendsen, H. J. C. (1977) Numerical integration of the Cartesian equations of motion of a system with constraints: Molecular dynamics of n-alkanes, *J. Comput. Phys. 23*, 327−341.
43. Meagher, K. L., and Carlson, H. A. (2005) Solvation Influences Flap Collapse in HIV-1 Protease, *Proteins: Struct. Funct. Bioinf. 58*, 119−125.
44. Berendsen, H. J. C., Postma, J. P. M., van Gunsteren, W. F., DiNola, A., and Haak, J. R. (1984) Molecular dynamics with coupling to an external bath, *J. Chem. Phys. 81*, 3684−3690.
45. Mongan, J. (2004) Interactive Essential Dynamics, *J. Comput.-Aided Mol. Des. 18*, 433−436.
46. Israilev, S., Stepaniants, S., Balsera, M., Oono, Y., and Schulten, K. (1997) Molecular dynamics study of unbinding of the avidin-biotin complex, *Biophys. J. 72*, 1568−1581.
47. Rose, R. B., Craik, C. S., and Stroud, R. M. (1998) Domain flexibility in retroviral proteases: Structural implications for drug resistance mutations, *Biochemistry 37*, 2607−2621.
48. Kurt, N., Scott, W. R. P., Schiffer, C. A., and Haliloglu, T. (2003) Cooperative Fluctuations of Unliganded and Substrate-Bound HIV-1 Protease: A Structure-Based Analysis on a Variety of Conformations From Crystallography and Molecular Dynamics Simulations, *Proteins: Struct. Funct. Genet. 51*, 409−422.
49. Wittayanarakul, K., Aruksakunwong, O., Saen-oon, S., Chantratita, W., Parasuk, V., Sompornpisut, P., and Hannongbua, S. (2005) Insights into saquinavir resistance in the G48V HIV-1 protease: Quantum calculations and molecular dynamic simulations, *Biophys. J. 88*, 867−879.
50. Wriggers, W., and Schulten, K. (1999) Investigating a Back Door Mechansim of Actin Phosphate Release by Steered Molecular Dynamics, *Proteins: Struct. Funct. Genet. 35*, 262−273.

BI700864P